J. Fluid Mech. (1993), *vol.* 257, *pp.* 559–574

Convection induced by inclined thermal and solutal gradients in a shallow horizontal layer of a porous medium

By D. A. NIELD[1], D. M. MANOLE[2] AND J. L. LAGE[2]

[1] Department of Engineering Science, University of Auckland, Auckland, New Zealand

[2] Mechanical Engineering Department, Southern Methodist University, Dallas, TX 75275-0335, USA

(Received 8 October 1992 and in revised form 23 June 1993)

A theoretical examination is made of convection, induced by applied thermal and solutal gradients inclined to the vertical, in a shallow horizontal layer of a saturated porous medium. The horizontal components of these gradients induce a Hadley circulation, which becomes unstable when the vertical components are sufficiently large. A linear stability analysis is carried out, and calculations are made using a low-order Galerkin approximation for the various modes of instability. The orientation of the preferred mode and the other critical quantities are determined for representative parameter values.

1. Introduction

A vast number of papers have been concerned with the natural convection, in a horizontal layer, induced by either horizontal or vertical temperature gradients, but very few have dealt with the more general situation of inclined temperature gradients. The case of convection in a viscous fluid has been treated by Weber (1973, 1978), Sweet, Jakeman & Hurle (1977), Bhattacharyya & Nadoor (1976) and Nadoor & Bhattacharyya (1981), and that of convection in a porous medium by Nield (1990, 1991). All these reports have been of theoretical investigations; as far as we are aware no experimental work has been published. The problem is complex. The results to date suggest that the differential equation system governing the flow will have, in general, multiple solutions. In view of this complexity, it is worthwhile to simplify the analysis by considering the flow in the central section of a shallow horizontal layer, one whose height-to-length and height-to-breadth ratios are small, so that the effect of lateral walls is to confine the fluid but it is otherwise negligible. The above publications have dealt, in fact, with this simplified problem, which we believe to be paradigmatic for more complicated problems.

In this paper the theoretical work is extended to the double-diffusive situation, where both thermal and solutal gradients are applied. Here we deal with convection in a saturated porous medium, and postpone a similar treatment of convection in a clear fluid. The former problem is simpler to deal with, because the differential equation system is of lower order. Also, comparison with future experimental work is more likely to be forthcoming. (It is extremely difficult to set up a uniform horizontal solutal gradient in a clear fluid, but there is a possibility of setting up one in a packed bed simultaneously with the assembly of the bed.) The double-diffusive problem treated in this paper is an extension (to inclined gradients) of the problem (for vertical gradients) which was first discussed by Nield (1968). Corrected results, together with a survey of

later work on double-diffusive convection in porous media, is contained in Nield & Bejan (1992, Chap. 9). A related paper is that of Sarkar & Phillips (1992). This deals with a thick layer and is concerned with the special case of zero horizontal density gradient and no Hadley flow. Sarkar & Phillips give references to a number of papers dealing with geological and environmental situations in which the thermohaline convection in a porous medium is applicable.

This paper is an extension of that by Nield (1990). We have found it convenient to introduce a novel scaling, so that the horizontal Rayleigh numbers appear explicitly in the boundary conditions for the governing equations. In order to rapidly explore a vast parameter space, we have been content to use a low-order Galerkin approximation, the order of accuracy of which has been determined in the previous work (Nield 1990). Even so, we have had to be narrowly selective in our choice of parameters used for computation, and we have considered only the case of Dirichlet-type boundary conditions on the perturbation temperature and concentration.

2. Basic equations

The situation considered is that illustrated in figure 1. The Cartesian axes are chosen with the z^*-axis vertically upwards. The superscript asterixes denote dimensional variables. The porous medium occupies a layer of height H. The vertical temperature difference across the boundaries is ΔT and the vertical concentration difference is ΔC. The imposed horizontal thermal and concentration gradient vectors are $(\beta_{T_x}, \beta_{T_y})$ and $(\beta_{C_x}, \beta_{C_y})$ respectively.

We assume that the Oberbeck–Boussinesq approximation is valid, and that flow in the porous medium is governed by Darcy's law. Accordingly the governing equations are

$$\nabla^* \cdot \boldsymbol{v}^* = 0, \tag{2.1}$$

$$0 = -\nabla^* P^* - (\mu/K)\,\boldsymbol{v}^* + \rho_f^* \boldsymbol{g}, \tag{2.2}$$

$$(\rho c)_m (\partial T^*/\partial t^*) + (\rho c_P)_f \boldsymbol{v}^* \cdot \nabla^* T^* = k_m \nabla^{*2} T^*, \tag{2.3}$$

$$\phi(\partial C^*/\partial t^*) + \boldsymbol{v}^* \cdot \nabla^* C^* = D_m \nabla^{*2} C^*, \tag{2.4}$$

$$\rho_f^* = \rho_0[1 - \gamma_T(T^* - T_0) - \gamma_C(C^* - C_0)]. \tag{2.5}$$

Here $(u^*, v^*, w^*) = \boldsymbol{v}^*$, P^*, T^* and C^* are the seepage (Darcy) velocity, pressure, temperature and concentration, respectively. The subscripts m and f refer to the porous medium and the fluid respectively. Also μ, ρ, and c denote the viscosity, density and specific heat, while K and ϕ are the permeability and porosity of the medium, k_m and D_m are the thermal and solutal diffusivities, and γ_T is the thermal expansion coefficient and γ_C the corresponding solutal quantity. (We prefer to maintain a symmetrical notation. Note that γ_C is normally a negative quantity.)

The boundary conditions are

$$\left.\begin{aligned} w^* = 0, \quad T^* &= T_0 - \tfrac{1}{2}(\pm\Delta T) - \beta_{T_x} x^* - \beta_{T_y} y^*, \\ C^* &= C_0 - \tfrac{1}{2}(\pm\Delta C) - \beta_{C_x} x^* - \beta_{C_y} y^* \quad \text{at} \quad z^* = \pm\tfrac{1}{2}H. \end{aligned}\right\} \tag{2.6}$$

We define non-dimensional quantities by

$$x = \frac{x^*}{H}, \quad t = \frac{\alpha_m t^*}{AH^2}, \quad (u, v, w) = \boldsymbol{v} = \frac{H\boldsymbol{v}^*}{\alpha_m},$$

$$P = \frac{K(P^* + \rho_0 g z^*)}{\mu\alpha_m}, \quad T = \frac{R_z(T^* - T_0)}{\Delta T}, \quad C = \frac{S_z(C^* - C_0)}{\Delta C},$$

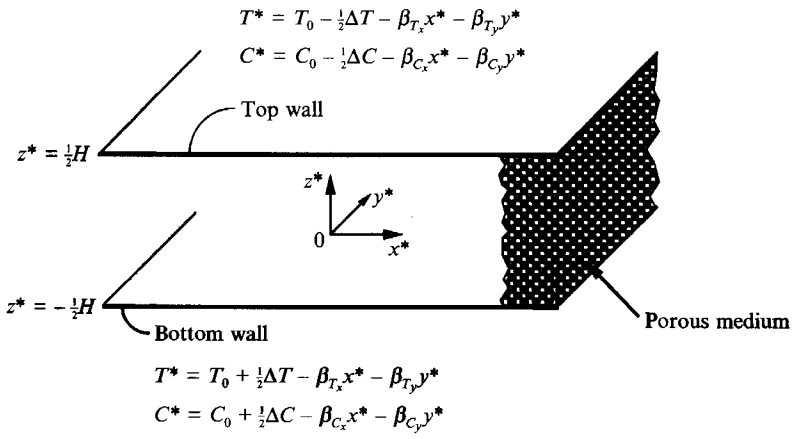

FIGURE 1. Sketch showing the geometry and the boundary conditions.

where $\alpha_m = \dfrac{k_m}{(\rho c_P)_f}$, $A = \dfrac{(\rho c)_m}{(\rho c_P)_f}$, $R_z = \dfrac{\rho_f g \gamma_T K H \Delta T}{\mu \alpha_m}$, $S_z = \dfrac{\rho_f g \gamma_C K H \Delta C}{\mu D_m}$.

We refer to R_z as the vertical thermal Rayleigh number and S_z as the vertical solutal Rayleigh number. In terms of the Lewis number $L_e = \alpha_m / D_m$ and the buoyancy ratio $N = \gamma_C \Delta C / \gamma_T \Delta T$ we have $S_z = N L_e R_z$. We also introduce the horizontal thermal and solutal Rayleigh numbers defined by

$$R_x = \frac{\rho_f g \gamma_T K H^2 \beta_{T_x}}{\mu \alpha_m}, \quad R_y = \frac{\rho_f g \gamma_T K H^2 \beta_{T_y}}{\mu \alpha_m},$$

$$S_x = \frac{\rho_f g \gamma_C K H^2 \beta_{C_x}}{\mu D_m}, \quad S_y = \frac{\rho_f g \gamma_C K H^2 \beta_{C_y}}{\mu D_m}.$$

The governing equations now take the form

$$\nabla \cdot \boldsymbol{v} = 0, \tag{2.7}$$

$$0 = -\nabla P - \boldsymbol{v} + (T + L_e^{-1} C)\boldsymbol{k}, \tag{2.8}$$

$$\partial T / \partial t + \boldsymbol{v} \cdot \nabla T = \nabla^2 T, \tag{2.9}$$

$$(\phi / A)\, \partial C / \partial t + \boldsymbol{v} \cdot \nabla C = L_e^{-1} \nabla^2 C. \tag{2.10}$$

The boundary conditions are now

$$\left.\begin{aligned} w &= 0, \\ T &= -\tfrac{1}{2}(\pm R_z) - R_x x - R_y y, \\ C &= -\tfrac{1}{2}(\pm S_z) - S_x x - S_y y \quad \text{at} \quad z = \pm \tfrac{1}{2}. \end{aligned}\right\} \tag{2.11}$$

We recognize that the scaling used for time and velocity is somewhat arbitrary in a double-diffusive context. It has the advantage that it puts (2.9) in its simplest form and groups ϕ and A together in (2.10). Our novel scaling of temperature and

concentration had the effect of making R_z and S_z appear in the boundary conditions rather than the differential equations, and this has the consequence that all the Rayleigh numbers appear in the perturbation equations via the steady-state solution only.

3. Steady-state solution

Equations (2.7)–(2.11) have a steady-state solution of the form

$$T_s = \tilde{T}(z) - R_x x - R_y y, \quad C_s = \tilde{C}(z) - S_x x - S_y y,$$
$$u_s = U(z), \quad v_s = V(z), \quad w_s = 0, \quad P_s = P(x, y, z).$$

This is a solution provided that

$$\mathrm{D}U = R_x + S_x/L_e, \quad \mathrm{D}V = R_y + S_y/L_e,$$
$$\mathrm{D}^2\tilde{T} = -UR_x - VR_y, \quad L_e^{-1}\mathrm{D}^2\tilde{C} = -US_x - VS_y.$$

Here D denotes the derivative operator, $\mathrm{d}/\mathrm{d}z$.

We suppose that there is no net flow in the horizontal direction, and so

$$\langle U \rangle = 0, \quad \langle V \rangle = 0,$$

where the angle brackets denote an average with respect to the vertical coordinate, which is equivalent to an integral with respect to z from $-\frac{1}{2}$ to $\frac{1}{2}$. One then obtains the solution

$$U = (R_x + S_x/L_e)\, z, \quad V = (R_y + S_y/L_e)\, z, \tag{3.1}$$

$$\tilde{T} = -R_z z + \tfrac{1}{24}\lambda_1 (z - 4z^3), \quad \tilde{C} = -S_z z + \tfrac{1}{24}\lambda_2 (z - 4z^3), \tag{3.2}$$

where

$$\lambda_1 = R_x^2 + R_y^2 + \frac{R_x S_x + R_y S_y}{L_e},$$

$$\lambda_2 = S_x^2 + S_y^2 + L_e(R_x S_x + R_y S_y). \tag{3.3}$$

The flow given by (3.1) is commonly referred to as a Hadley circulation.

We define the thermal and solutal Rayleigh number vectors by

$$\boldsymbol{R} = (R_x, R_y, R_z), \quad \boldsymbol{S} = (S_x, S_y, S_z).$$

We note that here the Hadley circulation is in the vertical plane containing the vector $\boldsymbol{R} + \boldsymbol{S}/L_e$.

4. Stability analysis

We now perturb the steady-state solution. We write

$$\boldsymbol{v} = \boldsymbol{v}_s + \boldsymbol{v}', \quad T = T_s + \theta', \quad C = C_s + c', \quad P = P_s + p'.$$

The linearized perturbation equations are

$$\nabla \cdot \boldsymbol{v}' = 0, \tag{4.1}$$

$$\nabla p' + \boldsymbol{v}' - (\theta' + c'/L_e)\boldsymbol{k} = 0, \tag{4.2}$$

$$\partial\theta'/\partial t + U\partial\theta'/\partial x + V\partial\theta'/\partial y - R_x u' - R_y v' + (\mathrm{D}\tilde{T})w' = \nabla^2\theta', \tag{4.3}$$

$$(\phi/A)\partial c'/\partial t + U\partial c'/\partial x + V\partial c'/\partial y - S_x u' - S_y v' + (\mathrm{D}\tilde{C})w' = L_e^{-1}\nabla^2 c'. \tag{4.4}$$

We make the normal mode expansion

$$[u', v', w', \theta', c', p'] = [u(z), v(z), w(z), \theta(z), c(z), p(z)]\exp\{\mathrm{i}(kx + ly - \sigma t)\}. \tag{4.5}$$

We substitute this into the perturbation equations and eliminate p, u and v from the resulting equations to obtain

$$(\mathrm{D}^2 - \alpha^2)w + \alpha^2\theta + \alpha^2 c/L_e = 0, \tag{4.6}$$

$$(\mathrm{D}^2 - \alpha^2 + \mathrm{i}\sigma - \mathrm{i}kU - \mathrm{i}lV)\theta + \mathrm{i}\alpha^{-2}(kR_x + lR_y)\mathrm{D}w - (\mathrm{D}\tilde{T})w = 0, \tag{4.7}$$

$$(L_e^{-1}[\mathrm{D}^2 - \alpha^2] + \mathrm{i}(\phi/A)\sigma - \mathrm{i}kU - \mathrm{i}lV)c + \mathrm{i}\alpha^{-2}(kS_x + lS_y)\mathrm{D}w - (\mathrm{D}\tilde{C})w = 0, \tag{4.8}$$

where $\alpha = (k^2 + l^2)^{\frac{1}{2}}$ is the overall horizontal wavenumber. We define the wavenumber vector by $\boldsymbol{\alpha} = (k, l, 0)$ and we refer to a disturbance with $\boldsymbol{\alpha}$ perpendicular to the direction of the Hadley circulation as a longitudinal mode. Similarly a disturbance with $\boldsymbol{\alpha}$ parallel to this plane will be called a transverse mode. For a longitudinal mode the flow is composed of convective rolls, with axes aligned with the Hadley circulation, superposed upon that circulation. For a transverse mode the roll axes are perpendicular to the Hadley circulation.

The last three equations must be solved subject to appropriate boundary conditions. For the case of impermeable, isothermal, isosolutal boundaries we have

$$w = \theta = c = 0 \quad \text{at} \quad z = \pm\tfrac{1}{2}. \tag{4.9}$$

The problem is now reduced to that of solving the equations (4.6)–(4.9) where

$$\mathrm{D}\tilde{T} = -R_z + \tfrac{1}{24}\lambda_1(1 - 12z^2), \quad \mathrm{D}\tilde{C} = -S_z + \tfrac{1}{24}\lambda_2(1 - 12z^2). \tag{4.10}$$

For the particular case of $L_e = \phi/A = 1$, the eigenvalue problem reduces to the same as for the monodiffusive case treated by Nield (1991), but with R_x, R_y, R_z replaced by $R_x + S_x$, $R_y + S_y$, $R_z + S_z$, (and with θ replaced by $\theta + c$).

In the general case, without loss of generality, we may regard R_z as the eigenvalue, with L_e, ϕ, A, R_x, R_y, S_x, S_y, S_z, σ, k and l as parameters. The critical value of R_z is its minimum as σ, k, l are varied (with σ taking certain determined values). Clearly we have a very large parameter space to explore, and any short cuts, such as the employment of approximate methods of calculation, are welcome.

5. Galerkin approximation

It is convenient to employ a low-order Galerkin approximation sufficiently accurate for the purpose in hand. We have found, by making spot comparisons of the results with those from a fourth-order approximation, that a second-order approximation appears to give values of the critical vertical Rayleigh number accurate to within about 1 % if λ_1 and λ_2 both have magnitudes less than 1000. The accuracy deteriorates rapidly for higher values of the magnitudes of λ_1 and λ_2. The main factor determining the accuracy appears to be the deviation from linearity of the basic thermal and solutal

profiles. The second-order approximation appears to be accurate whenever the applied vertical thermal and solutal gradients do not change sign as the vertical coordinate varies within the layer.

We select as trial functions (which satisfy the boundary conditions)

$$w_{2p-1} = \theta_{2p-1} = c_{2p-1} = \cos(2p-1)\pi z, \quad w_{2p} = \theta_{2p} = c_{2p} = \sin 2p\pi z$$
$$\text{for} \quad p = 1, 2, \ldots.$$

For the second-order approximation, for example, we put

$$w = A_1 w_1 + A_2 w_2, \; \theta = B_1 \theta_1 + B_2 \theta_2, \; c = C_1 c_1 + C_2 c_2$$

and substitute into the three equations (4.6)–(4.8). We multiply the first equation by w_1, the second by θ_1, the third by c_1, repeat the process with w_2, θ_2, c_2, then integrate each term with respect to z from $z = -\frac{1}{2}$ to $\frac{1}{2}$, perform some integrations by parts utilizing the boundary conditions, and eliminate the constants A_1, A_2, B_1, B_2, C_1 and C_2 from the resulting six homogeneous linear equations. We thus obtain the eigenvalue equation in the form

$$\det(A_{ij}) = 0, \tag{5.1}$$

where, for m, $n = 1, 2$,

$$\begin{aligned}
A_{3m-2,3n-2} &= \langle \mathrm{D}w_m \, \mathrm{D}w_n + \alpha^2 w_m \, w_n \rangle, \\
A_{3m-2,3n-1} &= -\alpha^2 \langle w_m \, \theta_n \rangle, \\
A_{3m-2,3n} &= -\alpha^2 L_e^{-1} \langle w_m \, c_n \rangle, \\
A_{3m-1,3n-2} &= \langle \mathrm{D}\tilde{T}\theta_m \, w_n - \mathrm{i}\alpha^{-2}(kR_x + lR_y)\,\theta_m \, \mathrm{D}w_n \rangle, \\
A_{3m-1,3n-1} &= \langle \mathrm{D}\theta_m \, \mathrm{D}\theta_n + (\alpha^2 - \mathrm{i}[\sigma - kU - lV])\,\theta_m \, \theta_n \rangle, \\
A_{3m-1,3n} &= 0, \\
A_{3m,3n-2} &= \langle \mathrm{D}\tilde{C}c_m \, w_n - \mathrm{i}\alpha^{-2}(kS_x + lS_y)\, c_m \, \mathrm{D}w_n \rangle, \\
A_{3m,n-1} &= 0, \\
A_{3m,3n} &= \langle L_e^{-1} \mathrm{D}c_m \, \mathrm{D}c_n + (L_e^{-1}\alpha^2 - \mathrm{i}[\phi\sigma/A - kU - lV])\, c_m \, c_n \rangle.
\end{aligned}$$

The various integrals involved are easily evaluated. For example, one obtains

$$\langle w_m \, w_n \rangle = \tfrac{1}{2}\delta_{mn}, \quad \langle Dw_m \, Dw_n \rangle = \tfrac{1}{2}m^2\pi^2\delta_{mn},$$

$$\langle z\theta_m \, w_n \rangle = \frac{4mn\nu_{mn}}{\pi^2(m^2-n^2)^2},$$

$$\langle z^2\theta_m \, w_n \rangle = \left(\frac{1}{24} - \frac{1}{4\pi^2 n^2}\right)\delta_{mn},$$

$$\langle \theta_m \, Dw_n \rangle = \frac{2mn\nu_{mn}}{n^2-m^2},$$

where

$$\nu_{mn} = \begin{cases} 0 & \text{if} \quad m+n \text{ is even}, \\ 1 & \text{if} \quad \tfrac{1}{2}(m+n+1) \text{ is even}, \\ -1 & \text{if} \quad \tfrac{1}{2}(m+n+1) \text{ is odd}. \end{cases}$$

Hence one finds that

$$A_{11} = \tfrac{1}{2}(\pi^2+\alpha^2), \quad A_{12} = -\tfrac{1}{2}\alpha^2, \quad A_{13} = -\tfrac{1}{2}L_e^{-1}\alpha^2, \quad A_{14} = A_{15} = A_{16} = 0,$$
$$A_{21} = -\tfrac{1}{2}R_z+\lambda_1/8\pi^2, \quad A_{22} = \tfrac{1}{2}(\pi^2+\alpha^2-\mathrm{i}\sigma), \quad A_{23} = 0,$$
$$A_{24} = -4\mathrm{i}\boldsymbol{\alpha}\cdot\boldsymbol{R}/3\alpha^2, \quad A_{25} = -8\mathrm{i}\{\boldsymbol{\alpha}\cdot\boldsymbol{R}+L_e^{-1}\boldsymbol{\alpha}\cdot\boldsymbol{S}\}/9\pi^2, \quad A_{26} = 0,$$
$$A_{31} = -\tfrac{1}{2}S_z+\lambda_2/8\pi^2, \quad A_{32} = 0, \quad A_{33} = \tfrac{1}{2}\{L_e^{-1}(\pi^2+\alpha^2)-\mathrm{i}\phi\sigma/A\},$$
$$A_{34} = -4\mathrm{i}\boldsymbol{\alpha}\cdot\boldsymbol{S}/3\alpha^2, \quad A_{35} = 0, \quad A_{36} = 8\mathrm{i}\{\boldsymbol{\alpha}\cdot\boldsymbol{R}+L_e^{-1}\boldsymbol{\alpha}\cdot\boldsymbol{S}\}/9\pi^2,$$
$$A_{41} = A_{42} = A_{43} = 0, \quad A_{44} = \tfrac{1}{2}(4\pi^2+\alpha^2), \quad A_{45} = -\tfrac{1}{2}\alpha^2, \quad A_{46} = -L_e^{-1}\alpha^2,$$
$$A_{51} = 4\mathrm{i}\boldsymbol{\alpha}\cdot\boldsymbol{R}/3\alpha^2, \quad A_{52} = 8\mathrm{i}\{\boldsymbol{\alpha}\cdot\boldsymbol{R}+L_e^{-1}\boldsymbol{\alpha}\cdot\boldsymbol{S}\}/9\pi^2, \quad A_{53} = 0,$$
$$A_{54} = -\tfrac{1}{2}R_z+\lambda_1/32\pi^2, \quad A_{55} = \tfrac{1}{2}(4\pi^2+\alpha^2-\mathrm{i}\sigma), \quad A_{56} = 0,$$
$$A_{61} = 4\mathrm{i}\boldsymbol{\alpha}\cdot\boldsymbol{S}/3\alpha^2, \quad A_{62} = 0, \quad A_{63} = 8\mathrm{i}\{\boldsymbol{\alpha}\cdot\boldsymbol{R}+L_e^{-1}\boldsymbol{\alpha}\cdot\boldsymbol{S}\}/9\pi^2,$$
$$A_{64} = -\tfrac{1}{2}S_z+\lambda_2/32\pi^2, \quad A_{65} = 0, \quad A_{66} = \tfrac{1}{2}\{L_e^{-1}(4\pi^2+\alpha^2)-\mathrm{i}\phi\sigma/A\}.$$

6. Analytical estimates

In general, it is impractical to solve (5.1) analytically, but this can be done for one special case. If $\boldsymbol{R}$ and $\boldsymbol{S}$ lie in the same vertical plane, then for the longitudinal modes one has $\boldsymbol{\alpha}\cdot\boldsymbol{R} = \boldsymbol{\alpha}\cdot\boldsymbol{S} = 0$, and the sixth-order determinant factorizes into the product of two third-order determinants, and the eigenvalue equation splits into two equations, one corresponding to an even mode (the eigenfunction being an even function of z) and the other to an odd mode. These modes can be then dealt with separately. The real and imaginary parts of the eigenvalue equation yield two equations, involving real quantities, to be solved simultaneously. One finds that there are two alternatives:

(i) $$\sigma = 0 \quad \text{and} \quad R_z+S_z-(\lambda_1+\lambda_2)/4\pi^2 = (\pi^2+\alpha^2)^2/\alpha^2; \tag{6.1}$$

or

(ii) $$(\phi L_e/A)\sigma^2 = (\pi^2+\alpha^2)^2-\alpha^2[R_z+S_z-(\lambda_1+\lambda_2)/4\pi^2] \tag{6.2}$$

and

$$(\phi L_e/A)(R_z-\lambda_1/4\pi^2)+(S_z-\lambda_2/4\pi^2) = [1+\phi L_e/A](\pi^2+\alpha^2)^2/\alpha^2. \tag{6.3}$$

As α varies, the minimum value of $(\pi^2+\alpha^2)^2/\alpha^2$ is $4\pi^2$, attained when $\alpha = \pi$. It follows that the neutral stability curve for the non-oscillatory (stationary, direct, monotonic are synonyms used) modes is given by

$$R_z+S_z = 4\pi^2+(\lambda_1+\lambda_2)/4\pi^2, \tag{6.4}$$

and that for the oscillatory modes is given by

$$(\phi L_e/A)(R_z-\lambda_1/4\pi^2)+(S_z-\lambda_2/4\pi^2) = 4\pi^2[1+\phi L_e/A]. \tag{6.5}$$

We recognize that these are the same as for the vertical-gradients case (cf. Nield & Bejan 1992, p. 278) but with R_z and S_z replaced by $R_z-\lambda_1/4\pi^2$ and $S_z-\lambda_2/4\pi^2$ respectively.

The second factor corresponds to the second lowest eigenvalue (for the vertical Rayleigh number), and yields the same results but with $4\pi^2$ replaced by $16\pi^2$.

For the case $\lambda_1 = \lambda_2 = 0$ these results are exact. For the general case they are only approximate, and, as we shall see below, the longitudinal modes are not always the favoured ones. Thus (6.4), (6.5) provide only upper bounds on the critical vertical Rayleigh number, for the coplanar case that we are considering.

7. Numerical calculations

7.1. *Procedure*

We decided that it was meaningful to work in terms of polar coordinates for the horizontal vectors, so we also made the transformations

$$\left.\begin{aligned} &k = \alpha\cos\Psi, \quad l = \alpha\sin\Psi, \\ &R_x = R_H\cos\Psi_R, \quad R_y = R_H\sin\Psi_R, \quad S_x = S_H\cos\Psi_S, \quad S_y = S_H\sin\Psi_S. \end{aligned}\right\} \tag{7.1}$$

The real and imaginary parts of (5.1) give a pair of equations which determine (R_z, σ) as functions of the nine parameters α, Ψ, R_H, Ψ_R, S_H, Ψ_S, S_z, A/ϕ and L_e. We were faced with the task of minimizing the value of R_z as (α, Ψ) varied with the other parameters held constant. In the present investigation we used the fixed values $L_e = 10$, $A/\phi = 1$. (This Lewis number is roughly representative for experiments with a sugar/salt system. The heat capacity/porosity ratio, A/ϕ, affects only the oscillatory modes. The value chosen for A/ϕ is also appropriate for that system.) Without loss of generality, the direction of the x^*-axis was chosen so that Ψ_S was always zero. Thus all orientations are now relative to the direction of the horizontal solutal gradient. For Ψ_R we selected the representative values 0°, 45°, 90°, 135° and 180°. We selected S_z values in the range $-100 \leqslant S_z \leqslant 100$, and restricted the value of R_H and S_H to those for which the second-order Galerkin approximation gives useful results.

We have written two programs to compute R_z. The first employed Gaussian elimination to calculate the determinant. This was used for the estimation of accuracy of the second-order approximation. The second was a special program for dealing efficiently with the second-order calculation only. The algorithm that was used capitalized on the fact that the determinant was quadratic in R_z and quartic in σ. *Mathematica* was employed to expand the determinant and write the resulting expression as a polynomial in R_z, whose coefficients were polynomials in σ, whose coefficients were powers of α^2. The algebraic expressions for the roots of the R_z quadratic equation were then put into a Fortran program and evaluated using double precision. For each evaluation of an R_z root the values of σ were sought to ensure that $\mathrm{Im}(R_z)$ were zero. (We utilized the fact that $\mathrm{Im}(R_z)$ is a fourth-degree polynomial in σ.) For each such value of σ the wavenumber parameters α, Ψ were varied to give the minimum value of $\mathrm{Re}(R_z)$. The least of these minima is the critical value of R_z.

The expressions for R_z are periodic in Ψ, with period 180°, and this allowed us to restrict the calculations to the interval $0° \leqslant \Psi \leqslant 180°$. For the case $\Psi_R = 0$, i.e. when the thermal and solutal gradients are coplanar, there is a further symmetry which allowed a restriction to the interval $0° \leqslant \Psi \leqslant 90°$. After locating the region containing the absolute minimum of R_z, we determined the minimum using a step size that was typically 0.1° for Ψ and 10^{-6} for α, and, for the oscillatory modes, we determined σ to within 10^{-6}. Hence the numerical inaccuracy is much less than the inaccuracy arising from the Galerkin approximation.

7.2. *Results*

We first present, in figure 2, some values of the critical thermal vertical Rayleigh number, R_z, as a function of R_H and S_H, for the case $S_z = 0$ and $\Psi_R = 0°$ or 180° (the

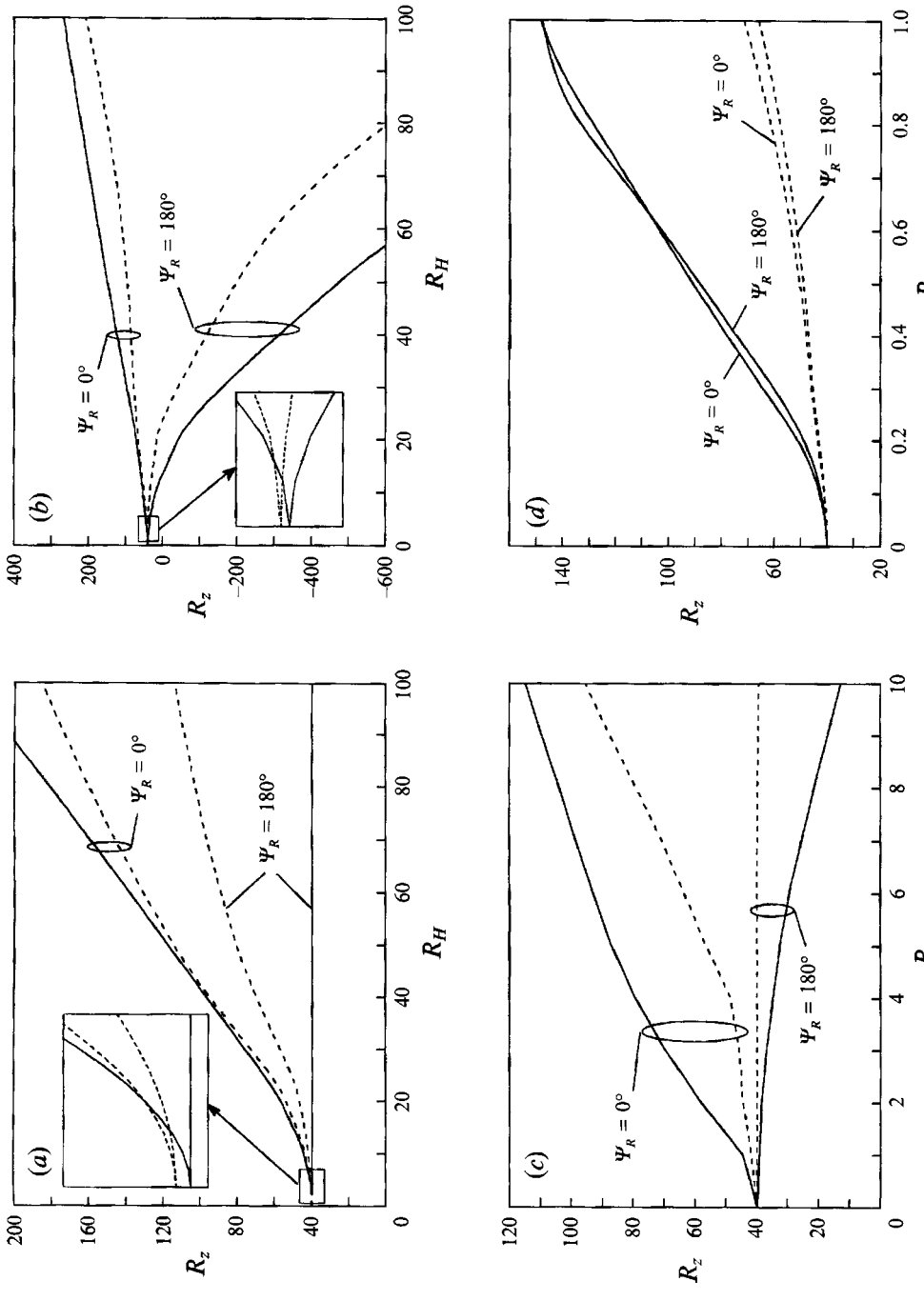

FIGURE 2. Critical vertical thermal Rayleigh number for the oscillatory (dashed lines) and non-oscillatory (continuous lines) modes. $S_z = 0$, and $\Psi_R = 0$ or 180° (coplanar case). (*a*) $S_H = R_H/L_e$, (*b*) $S_H = R_H$, (*c*) $S_H = L_e R_H$, (*d*) $S_H = L_e^2 R_H$.

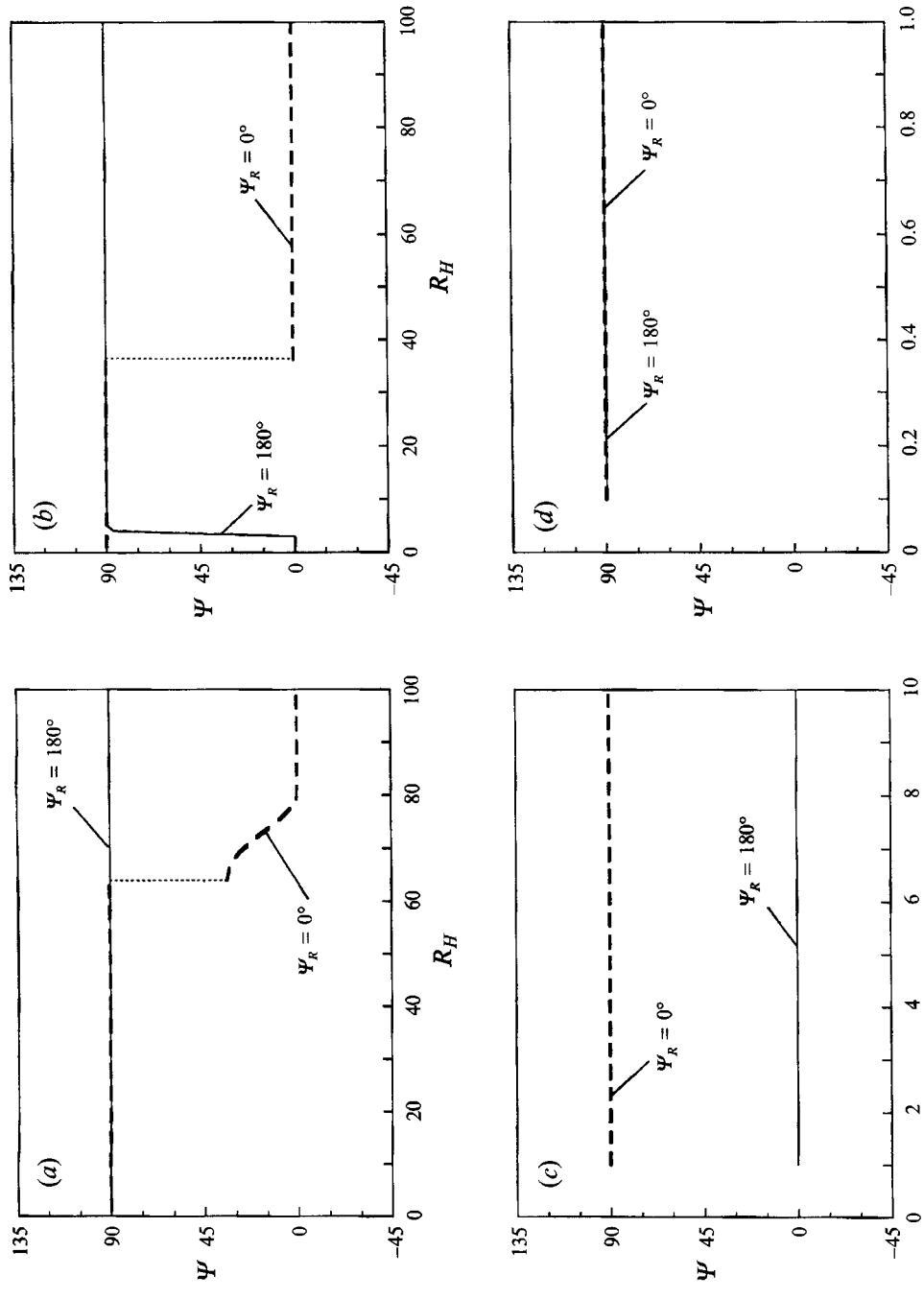

FIGURE 3. Orientation of the preferred modes. $S_z = 0$, $\Psi_R = 0$ or 180° (coplanar case). (*a*) $S_H = R_H/L_e$, (*b*) $S_H = R_H$, (*c*) $S_H = L_e R_H$, (*d*) $S_H = L_e^2 R_H$.

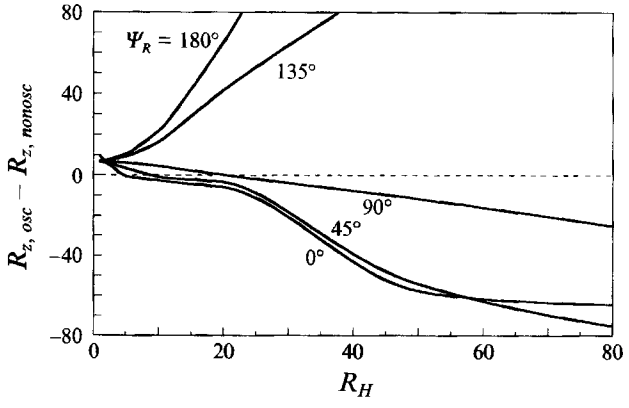

FIGURE 4. Comparison of the critical vertical Rayleigh numbers for the oscillatory and non-oscillatory modes, for various orientations of the horizontal thermal Rayleigh number vector. $S_z = 10$, $R_H = S_H$.

coplanar case). The values for a non-oscillatory mode are plotted as a continuous line and those for an oscillatory mode as a dashed line. Each graph shows two pairs of curves, each pair pertaining to a certain value of S_H/R_H. The four sets of values are 0.1 ($= 1/L_e$), 1, 10 ($= L_e$), and 100 ($= L_e^2$), respectively. The corresponding values of Ψ, giving the orientation of the preferred modes, are plotted in figure 3. Because we consider them of lesser interest, we have not presented the corresponding values of α and σ. (We mention that, providing R_H and S_H are less than about 80, the critical value of α does not vary much from 3.1, the value of $S_H = R_H = 0$. At larger values of R_H and S_H there can be a dramatic change in α, corresponding to a transition from an even mode to an odd one, as noted by Nield (1991).)

Figure 4 presents, for the representative value $S_z = 10$ and for $R_H = S_H$, the difference between the minimum R_z for the oscillatory mode and that for the non-oscillatory mode, for five different orientations of the horizontal thermal Rayleigh number vector, namely for $\Psi_R = 0°$, 45°, 90°, 135° and 180°. Above the dashed line the preferred mode is non-oscillatory and below this line the preferred mode is oscillatory. The figure shows that the non-oscillatory mode is preferred for $\Psi_R > 90°$ while the oscillatory mode is preferred for $\Psi_R < 90°$.

The relative influence of R_H and S_H was investigated by keeping $S_H = 10$ and varying $R_H = 1, 10, 100$. The effect of varying S_z was similarly investigated. The graphs in figure 5, for $\Psi_R = 0°$ (*a*) and 180° (*b*), show the critical R_z for the non-oscillatory (continuous line) and oscillatory (dashed line) modes. The value of S_z at the transition between oscillatory and non-oscillatory modes increases for both cases when R_H is increased. (Note that the result for $\Psi_R = 180°$ can be deduced from that for $\Psi_R = 0°$ by formally replacing R_H by $-R_H$.)

We now concentrate on the case $R_H = S_H = 10$, values for which our second-order scheme gives highly accurate results, and investigate the effect of varying the orientation of the horizontal thermal gradient as well as S_z. The results for $\Psi_R = 0°$ and 180° have already been depicted by the thick lines in figure 5. The corresponding results for $\Psi_R = 45°$ and 135° are exhibited in figure 6. The chief feature is that the preferred mode switches from oscillatory to non-oscillatory as S_z increases.

Figure 7 shows how the orientation Ψ of the preferred critical mode varies with S_z, for the five orientations of R_H. A cross denotes the location of the transition point between the oscillatory and the non-oscillatory modes. It is noteworthy that over a

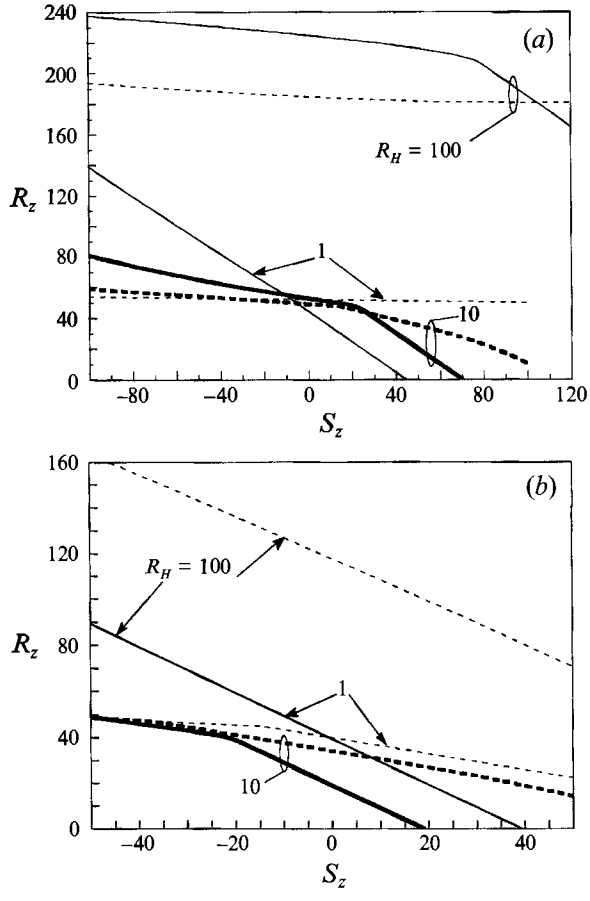

FIGURE 5. Effect of the amplitude of the horizontal thermal Rayleigh number vector on the stability boundaries for oscillatory modes (dashed lines) and non-oscillatory modes (continuous lines). $S_H = 10$. (*a*) $\Psi_R = 0°$, (*b*) $\Psi = 180°$.

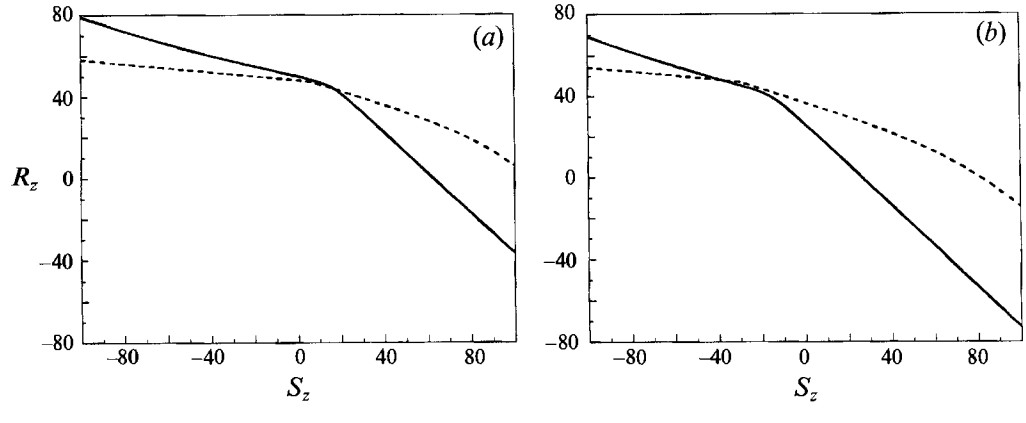

FIGURE 6. Effect of the orientation of the horizontal thermal Rayleigh number vector on the transition from oscillatory (dashed lines) to non-oscillatory (continuous lines) modes. $S_H = R_H = 10$. (*a*) $\Psi = 45°$, (*b*) $\Psi = 135°$.

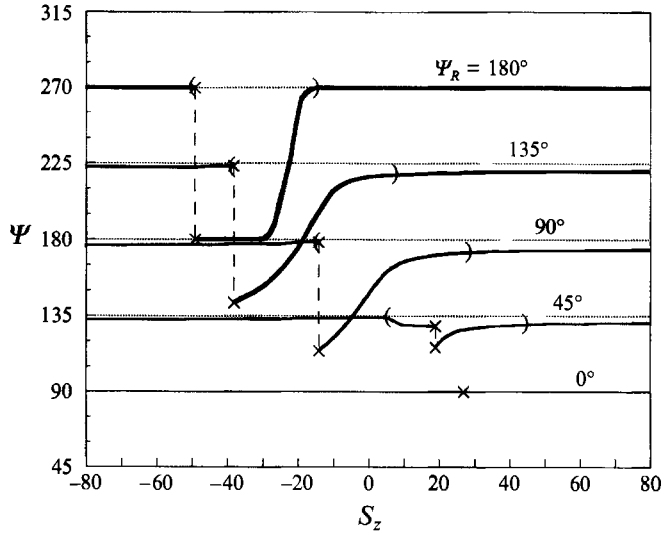

FIGURE 7. Orientation of the preferred modes. Parentheses delimit regions of oblique modes. Crosses indicate transition from oscillatory to non-oscillatory modes. $S_H = R_H = 10$.

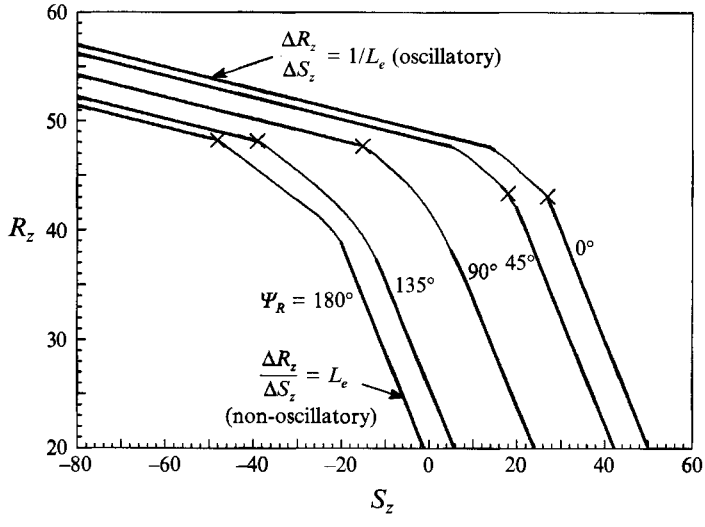

FIGURE 8. Overall stability boundaries for various orientations of the horizontal thermal Rayleigh number vector. $S_H = R_H = 10$.

wide range of S_z one has the relation $\Psi \approx \Psi_F + 90°$, where Ψ_F, which gives the orientation of the basic flow, is given according to (3.1) by

$$\Psi_F = \tan^{-1}(V/U) = \tan^{-1}[(R_y + S_y/L_e)/(R_x + S_x/L_e)]. \tag{7.2}$$

(For the cases presented in figure 7 it turns out that $\Psi_F \approx \Psi_R$.) This means that the preferred mode is almost longitudinal to the basic flow except within the regions delimited by the parentheses in the figure; in these regions oblique modes are preferred. The amount of variation inside such a region increases with Ψ_R, from zero at $\Psi_R = 0°$ to 90° at $\Psi_R = 180°$. The dashed lines linking the transition points, denoted by the crosses, have been inserted solely to facilitate the perception of the curves.

In order to obtain a global picture of the critical Rayleigh numbers, we show in

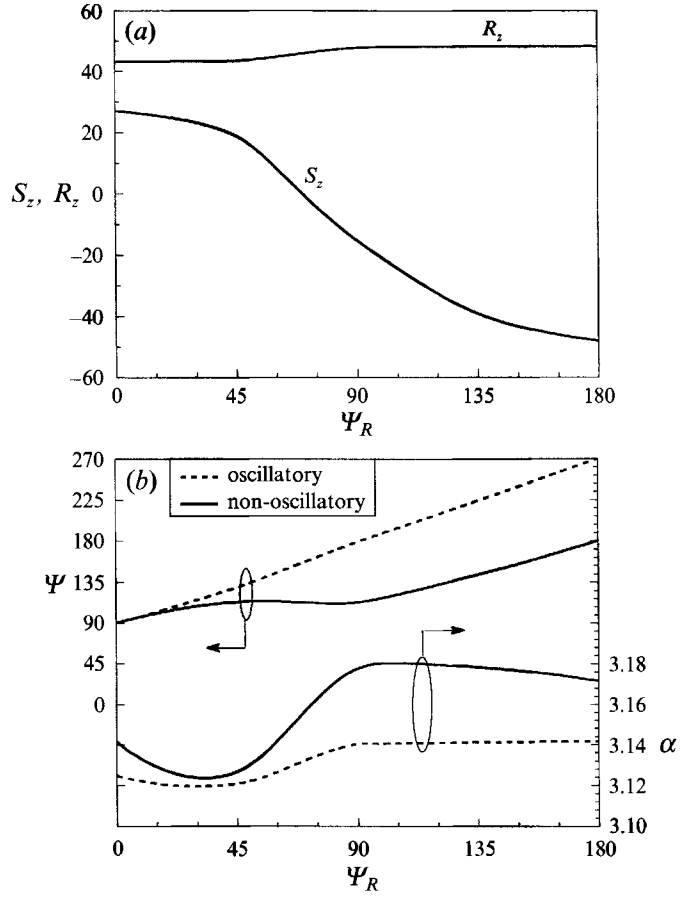

FIGURE 9. Data for the transition between oscillatory and non-oscillatory modes. $S_H = R_H = 10$.

figure 8 the overall critical R_z, i.e. the smaller of the oscillatory and non-oscillatory values of R_z, as a function of S_z. We note three regimes. For large negative values of S_z the preferred mode is oscillatory and the slope of the line has constant magnitude L_e^{-1}. For large positive values of S_z the preferred mode is non-oscillatory and the slope has constant magnitude L_e. For intermediate values of S_z, where the curves are drawn thinner, the variation is not linear. Again a cross denotes the transition point between the oscillatory and non-oscillatory modes.

Figure 9 presents as functions of Ψ_R, values pertaining to the transition point. Figure 9(*a*) shows the values of R_z and S_z while figure 9(*b*) presents the critical wavenumber parameters α and Ψ at the transition point, for each of the oscillatory and non-oscillatory modes.

8. Discussion

The gross features of figure 2, illustrating the coplanar situation, are in accord with our expectation. With reference to figure 1, and using thermohaline terminology, we always have fresh water on the left and salty water on the right, since we have made S_x positive. If R_x is also positive ($\Psi_R = 0$) then we have hot water on the left and cold water on the right. The steady-state density then increases from left to right and, in accordance with (3.1), the direction of the basic circulation is that the hotter fresher

water flows above cooler denser water, a stable situation. One would therefore expect that the effect of the horizontal gradients would be stabilizing, i.e. to increase the critical vertical Rayleigh number R_z, and this is borne out by the results shown in figure 2.

On the other hand, when R_x is negative ($\Psi_R = 180°$) we have cold fresh water on the left and hot salty water on the right. The density gradient is in the positive (or negative) x-direction according as $S_H > L_e R_H$ (or $S_H < L_e R_H$), respectively. Again in accordance with (3.1), when $S_H < L_e R_H$ we have hotter saltier water flowing (to the left) over cooler fresher water. This is the unstable situation associated with fingering, and we expect the effect of the horizontal gradients to cause increased instability (of the non-oscillatory kind) Again this is borne out by our figure. The case of $S_H = L_e R_H$ corresponds to steady-state isodensity in the horizontal direction, and no Hadley flow. (This is the situation studied by Sarkar & Phillips 1992.) Our results show that in this case the effect of the horizontal gradients is again to cause increased non-oscillatory instability.

Particularly interesting is the prediction that the horizontal gradients can cause instability in the absence of any vertical gradients. This result is in accord with the study of the clear-fluid case by Thorpe, Hutt & Soulsby (1969). We confirm their conclusion (based on a Squire's theorem type of argument) that the preferred mode is transverse, and their conjecture that the preferred mode is non-oscillatory in such circumstances. (We offer the following physical explanation. A fluid particle displaced to the right finds itself in a hotter, saltier environment. Because of the large diffusivity of heat it warms up quickly. It is then less dense than its surroundings and so is subject to an upwards buoyancy force. Similarly a particle displaced to the left is subject to a downwards buoyancy force. The net effect is a tendency to produce vorticity in the negative y-direction. If this tendency is sufficiently large – and this is so when R_H is sufficiently large – to overcome the retarding effect of viscosity, then a Hadley circulation can be induced, but this in turn is unstable to cellular motion (non-oscillatory) because hotter saltier water is flowing above cooler fresher water.)

Finally, when $S_H > L_e R_H$ we have cooler fresher water flowing (this time to the right) over hotter saltier water, and we expect increased instability of the oscillatory type. Our expectation is only partly confirmed. The oscillatory mode is indeed generally favoured, but the effect of the horizontal gradients is generally stabilizing.

In the monodiffusive case it was found (Nield 1991) that the non-oscillatory longitudinal mode was invariably the preferred mode. (We recall that, as defined in §4, a longitudinal mode is characterized by $k = 0$ or, equivalently, $\Psi = 90°$.) From figure 3 we see that in the double-diffusive case the preferred mode can be longitudinal, transverse, or oblique, depending on the parameters.

Figure 4 indicates that generally an oscillatory mode is preferred to a non-oscillatory one when the horizontal thermal and solutal gradients make an acute angle with each other, and this is because (see figure 2) the oscillatory mode is stabilized (by the horizontal gradients) to a lesser extent than is the non-oscillatory mode. The non-oscillatory mode is preferred when the horizontal thermal and solutal gradients make an obtuse angle with each other because the oscillatory mode is destabilized to a lesser extent than is the non-oscillatory mode.

The general form of the stability curves in the (S_z, R_z)-plane is in general accord with expectations based on the well-known results for the vertical gradients case and the trend of the analytical results of §6. The curves are generally concave towards the origin, indicating less than perfect coupling between the two agencies (vertical thermal and solutal gradients) causing the instability. (A straight line indicates perfect coupling.) As S_z tends to plus infinity each curve asymptotes to a line with slope -1

and the instability is non-oscillatory (compare (6.4)). As S_z tends to minus infinity each curve asymptotes to a line with slope $-L_e^{-1}$, for the case $(\phi/A = 1)$ for which calculations have been made, and the instability is oscillatory. More generally (see (6.5)) the oscillatory stability curve will have an asymptote with slope $-A(\phi L_e)^{-1}$. The effect of horizontal gradients does make one major difference. In the vertical-gradients case the oscillatory stability boundary bifurcates from the non-oscillatory boundary and the frequency σ has a cut-off at this point. In the inclined-gradients case the curves in the (S_x, R_x)-plane just cross each other (they are the projections of bifurcation surfaces) and we do not observe any frequency cut-off.

Sarkar & Phillips (1992) have distinguished between 'double-advective' and 'double-diffusive' instability in a porous medium. We prefer to speak of the 'hetero-advective' and 'iso-advective' types of double-diffusive instability. The first applies to a thermohaline system. Heat is advected with the Darcy (seepage) velocity $\boldsymbol{v}$, but salt is advected with the intrinsic velocity, $\boldsymbol{v}/\phi$, because salt (and any other solute) cannot pass through the solid part. The consequences can be seen by comparing (2.3) with (2.4), or (2.9) with (2.10), and parallel equations for another solute. (Note that $D_m = \phi D$, where D is the solutal diffusivity in a clear fluid.) The iso-advective system formally corresponds to the value 1 for ϕ/A, the value that we selected for our calculations. Changing to a more general value of ϕ/A does not affect our results for the non-oscillatory modes, but it does affect those for the oscillatory modes, notably in the manner mentioned in the previous paragraph.

When experimental results are available it will be worthwhile to extend the calculations to other values of the parameters. In the meantime we believe that our results should serve as a useful guide.

J.L.L. and D.M.M. would like to acknowledge with gratitude the support from the School of Engineering and Applied Sciences of the Southern Methodist University. D.A.N. benefitted from helpful discussions with R. I. Nokes. We are grateful to the United States – New Zealand Cooperative Science Program for help in initiating our collaboration.

REFERENCES

BHATTACHARYYA, S. P. & NADOOR, S. 1976 Stability of thermal convection between non-uniformly heated plates. *Appl. Sci. Res.* **32**, 555–570.

FINLAYSON, B. A. 1972 *The Method of Weighted Residuals and Variational Principles*. Academic.

NADOOR, S. & BHATTACHARYYA, S. P. 1981 Hydromagnetic thermal convection between non-uniformly heated plates. *Acta Mech.* **41**, 265–282.

NIELD, D. A. 1968 Onset of thermohaline convection in a porous medium. *Water Resources Res.* **11**, 553–560.

NIELD, D. A. 1990 Convection in a porous medium with inclined temperature gradient and horizontal mass flow. In *Heat Transfer 1990*, vol. 5, pp. 153–158. Hemisphere.

NIELD, D. A. 1991 Convection in a porous medium with inclined temperature gradient. *Intl J. Heat Mass Transfer* **34**, 87–92.

NIELD, D. A. & BEJAN, A. 1992 *Convection in Porous Media*. Springer.

SARKAR, A. & PHILLIPS, O. M. 1992 Effects of horizontal gradients on thermohaline instabilities in a thick porous layer. *Phys. Fluids* A **4**, 1165–1175.

SWEET, D., JAKEMAN, E. & HURLE, D. T. J. 1977 Free convection in the presence of both vertical and horizontal temperature gradients. *Phys. Fluids* **20**, 1412–1415.

THORPE, S. A., HUTT, P. K. & SOULSBY, R. 1969 The effect of horizontal gradients on thermohaline convection. *J. Fluid Mech.* **38**, 375–400.

WEBER, J. E. 1973 On thermal convection between non-uniformly heated planes. *Intl J. Heat Mass Transfer* **16**, 961–970.

WEBER, J. E. 1978 On the stability of thermally driven shear flow heated from below. *J. Fluid Mech.* **87**, 65–84.